



## Simulation of three-dimensional circulation and hydrography over the Grand Banks of Newfoundland

Guoqi Han<sup>a,b,\*</sup>, Zhimin Ma<sup>b</sup>, Brad deYoung<sup>b</sup>, Mike Foreman<sup>c</sup>, Nancy Chen<sup>a</sup>

<sup>a</sup> Biological and Physical Oceanography Section, Fisheries and Oceans Canada, Northwest Atlantic Fisheries Centre, St. John's, NL, Canada

<sup>b</sup> Department of Physics and Physical Oceanography, Memorial University of Newfoundland, St. John's, NL, Canada

<sup>c</sup> Institute of Ocean Science, Fisheries and Oceans Canada, Sydney, BC, Canada

### ARTICLE INFO

#### Article history:

Received 2 February 2011

Received in revised form 23 August 2011

Accepted 27 August 2011

Available online 10 September 2011

#### Keywords:

Shelf circulation

Labrador Current

Temperature

Salinity

Tides

Numerical modeling

Grand Banks of Newfoundland

### ABSTRACT

There are few ocean models that both adequately resolve the cross-shelf structure of the Labrador Current and have been sufficiently evaluated against *in situ* observations at tidal, synoptic and seasonal scales. We present a three-dimensional, high-resolution, prognostic, nonlinear circulation model for the Newfoundland offshore based on the finite volume coastal ocean model (FVCOM). The FVCOM uses unstructured grid in the horizontal and thus allows efficient and effective use of grid resolution to resolve coastal- and shelf-scale features. The model results are evaluated against current meter measurements, vessel-mounted acoustic Doppler current profiler (ADCP) data, and tide-gauge observations. The FVCOM climatological monthly-mean currents over the shelf and slope show good agreement with observations and substantial improvement over those from an earlier finite-element model. The simulated tidal elevations agree well (4 cm of the root-sum-square absolute error for the total tidal height) with observations, and show improvement over previous tidal models over the Labrador Shelf. The hindcasts for the spring to fall of 1999 show reasonable skill in reproducing temperature, salinity and currents. At station 27 the observed temperature and salinity have seasonal ranges of 14 °C and 1.5 psu near the surface from April to November; while the root-mean-square (RMS) differences are 2.1 °C and 0.3 psu between the model and observations. On the Flemish Cap transect the observed temperature and salinity range from −1.5 to 13.1 °C and from 31.3 to 34.9 psu on July 17–20, 1999; while the RMS differences are 1.0 °C and 0.2 psu. The model-observation velocity difference ratio is 0.53 on this transect on July 17–18, 1999.

Crown Copyright © 2011 Published by Elsevier Ltd. All rights reserved.

### 1. Introduction

The Grand Banks of Newfoundland are located at a pivotal point of the world climate system, one of the few locations subject to the impacts of the Arctic outflows, and one of the most important regions for the tropical-polar heat exchanges and for shelf and deep-ocean interactions. It is also one of the most productive areas in the global marine ecosystem. With the influence of different water masses from the colder fresher Labrador Current water, the slightly warmer and saltier Labrador Sea water and the warm and salty Gulf Stream water, physical and biological ocean environments in the Newfoundland waters are highly complex and variable (sensitive to climate variability and change), and have profound effects on the regional ecosystem (Han and Kulka, 2009), including numerous coastal embayments. Ocean currents and associated hydrographic conditions are important to, and at

times control the transport and survival of the eggs and larvae of marine organisms (Pepin and Helbig, 1997; Han and Kulka, 2009). While *in situ* observations have been the primary avenue for knowledge of the regional physical oceanography, ocean modeling has become increasingly important in providing accurate and timely information on physical oceanographic conditions to address issues related to fisheries, aquaculture, navigation, search and rescue, environment, and marine energy.

Modeling studies prior to the 2000s for this region focused on structured-grid ocean models based on the finite-difference method. Greenberg and Petrie (1988) developed a barotropic ocean model for the Grand Bank of Newfoundland, showing the detailed structure in the mean circulation. Tang et al. (1996) established a 3-D diagnostic model for the Newfoundland and Labrador Shelves, providing 3-D seasonal baroclinic circulation features. Han (2000) set up a 3-D barotropic tide model, showing substantial variability of tidal currents and associated mixing over the Grand Bank and its vicinity. Coupled ice-ocean models were developed off Newfoundland and Labrador (Yao et al., 2000) and for the eastern Canadian shelf (Zhang et al., 2004), but without including tidal dynamics.

\* Corresponding author at: Biological and Physical Oceanography Section, Fisheries and Oceans Canada, Northwest Atlantic Fisheries Centre, St. John's, NL, Canada. Tel.: +1 709 772 4326; fax: +1 709 772 4188.

E-mail address: [guoqi.han@dfp-mpo.gc.ca](mailto:guoqi.han@dfp-mpo.gc.ca) (G. Han).

While further efforts have been made in developing the finite-difference models (e.g. currently another regional operational ocean model of the Northwest Atlantic is under development by the Northwest Atlantic Fisheries Centre, Fisheries and Oceans Canada), a new thrust in the ocean modeling for the Grand Banks of Newfoundland since the late 1990s has been the development and application of unstructured-grid ocean models to barotropic and baroclinic circulation (e.g. Loder et al., 1997; Han et al., 1999). A linear finite-element model was developed to study seasonal and interannual wind-driven circulation off Newfoundland and Labrador (Han, 2005), revealing the importance of the large-scale wind-driven circulation in the Labrador Current. The study analyzed the barotropic wind-driven circulation pattern over the Newfoundland and Labrador Shelves, especially the significance of the North Atlantic wind forcing in the inshore, shelf-edge and deep-ocean branches of the Labrador Current. Recently, Han et al. (2008) presented a 3-D nonlinear, finite-element, baroclinic circulation model that sufficiently resolved the coastal and shelf-edge Labrador Current. The model climatological monthly-mean currents validated against *in situ* observations indicated significant contributions of both baroclinic and barotropic components to the seasonal mean circulation. However, the robust diagnostic method of their model does not allow full prognostic adjustment. Full prognostic models that resolve the Labrador Current and include major tides and synoptic atmospheric forcing are required. Among various promising state-of-the-art ocean models is the finite volume coastal ocean model (FVCOM), developed by Chen et al. (2003). The finite-volume approach is geometrically flexible (comparable to the finite element method), numerically simple and computationally efficient (comparable to the finite difference method).

In this study, we develop a three-dimensional prognostic model based on the FVCOM (Chen et al., 2003) for the Grand Banks of Newfoundland, to provide a new modeling capacity for this region. Our main objectives are: (1) to establish a high-resolution circulation model that can well resolve the inshore and offshore Labrador Current and can provide realistic, synoptic circulation fields for various ecosystem and environmental applications in the region; and (2) to generate realistic open boundary conditions for coastal embayment models along the South and East Newfoundland. In Section 2 we describe the model, boundary conditions, forcing data, initial conditions, and solution procedure. Section 3 discusses model-observation comparison and evaluation of the synoptic circulation and hydrography. Section 4 presents the evaluation at the tidal time scales and Section 5 at the climatological seasonal scale. We conclude with a brief summary and discussion in Section 6.

## 2. Circulation models, initial and open boundary conditions

### 2.1. FVCOM and mesh

The FVCOM model (Chen et al., 2003, 2006) used in this study consists of 3-D, nonlinear, primitive equations with Boussinesq and hydrostatic approximations and a level-2.5 turbulence closure scheme for vertical mixing. A mode-splitting technique is used to solve the momentum equations: an external barotropic mode for the free sea surface height and an internal baroclinic one for the 3-D velocity.

The model domain covers the southern Labrador Shelf (SLS), the Newfoundland Shelf, and extends over the adjacent deep ocean where the Gulf Stream and the North Atlantic Current are located. In the horizontal, the model has a linear triangular grid (Fig. 2) with 10,927 unequally spaced nodes where the sea level and other scalar variables are located and 21,046 elements with the velocities located at their centroid. The horizontal grid has a typical nodal

spacing of 5 km over the shelf, with high resolution for steep-slope areas near the coast and over the shelf edge (up to 1 km). In the vertical, the model has 21 non-uniform  $\sigma$  levels with a higher resolution near the sea surface and the seabed. The bottom topography includes the shelf topography (4' by 4' resolution) from the Canadian Hydrographic Service and the deep-ocean topography (5' by 5') from etopo5.

### 2.2. Model forcing and boundary conditions

The prognostic model is forced by temporally and spatially variable wind stresses and heat fluxes calculated from the 6-hourly atmospheric data in 1999. The wind velocity fields are  $0.25^\circ$  by  $0.25^\circ$  6-hourly scatterometer products from the US National Climatic Data Center (Zhang et al., 2006). Where there are no satellite wind data, the  $0.5^\circ$  by  $0.5^\circ$  model winds from the Canadian Meteorological Centre (CMC) are used. Wind stresses are calculated using the FVCOM piece-wise linear formula (Chen et al., 2006). Heat fluxes are calculated using a Matlab-based package including Pawlowicz et al. (2001) air-sea toolbox. The surface short wave flux is estimated using Curry and Webster's (1999) formulation. A revised function of Li et al. (2006) is used to calculate the albedo including the white cap effect (Monahan and MacNiocail, 1986). The function of Fung et al. (1984) is used to compute longwave radiation based on the monthly sea surface temperature climatology of Geshelin et al. (1999) and the air temperature, dew temperature, wind speed and cloud cover from the CMC's atmospheric model output. A modified TOGA COARE code (Fairall et al., 1996) is used to derive the sensible and latent heat fluxes. The calculated net heat flux and short wave radiation at the sea surface are interpolated to the nodal locations.

Temperature and salinity at the open boundary are interpolated from Geshelin et al.'s (1999)  $1/6^\circ$  by  $1/6^\circ$  Climatological, monthly-mean fields at each time step. The temperature and salinity at the open boundary are specified for the inflow and calculated by the model for the outflow. Zero normal gradients of temperature and salinity are enforced at the lateral land boundaries. Surface salinity is restored to the monthly-mean climatology at a time scale of 5 days, to implicitly account for, on the seasonal scale, the sea surface freshwater fluxes and buoyancy forcing associated with ice melting. At the sea floor, the normal gradient of temperature and salinity are set to zero.

Tidal heights for the five major semi-diurnal ( $M_2$ ,  $S_2$ , and  $N_2$ ) and diurnal ( $K_1$  and  $O_1$ ) constituents based on Han et al. (2010) are specified along the open boundaries. Non-tidal sea levels along the open boundaries are interpolated from the climatological monthly-mean sea level of Han et al. (2008). The monthly sea level includes steric height with the normal bottom velocity equal to zero, the large-scale wind effect, and the large-scale barotropic current, as described by Han et al. (2008). Zero normal velocity is specified at the coastal land boundaries.

### 2.3. Initial conditions

To shorten the prognostic model spin-up period, the model initial temperature, salinity, sea level, and currents conditions are constructed based on an average of the March and April climatological monthly-mean solutions of FVCOM. These climatological monthly-mean solutions themselves are obtained by using the NCEP-NCAR wind at the sea surface, the monthly-mean sea level, temperature and salinity, the five tidal constituents at the open boundary and by using the monthly temperature and salinity climatology of Geshelin et al. (1999) as the initial condition.

For the climatological monthly-mean runs, the sea surface temperature and salinity are restored to the monthly-mean climatology at a 12.42-h timescale (the  $M_2$  tidal period), to allow tidal-

scale dynamical adjustment. The model has external and internal time steps of 6.21 and 62.1 s, respectively. The model forcing is ramped up from zero to its full value over 41 h. For each month, the model was integrated forward from rest for 2 months until overall dynamic equilibrium is established. We then separate the tidal and mean fields using harmonic analysis based on the last 30-day model output.

#### 2.4. Solution procedure

The prognostic model was integrated continuously forward in time from the initial state generated in Section 2.3, by using the boundary conditions described in Section 2.2. The model has external and internal time steps of 6.21 and 62.1 s, respectively. The temperature and salinity below the 35-m (deeper than the mixed layer depth in summer) depth were nudged toward the monthly-mean climatology of Geshelin et al. (1999) at

a scale of 5 days. The model run starts on April 1, 1999 and is carried out for a total of 2 years under the same 1999 surface forcing.

### 3. Validation of the baseline prognostic model at sub-tidal time scales

To evaluate the model solutions qualitatively and quantitatively, we compare the model solutions with various measurements. In addition to the correlation coefficient and the root-mean-square (RMS) difference, we examine the velocity difference ratio (VDR) defined as the ratio of the sum of the squared magnitudes of the vector velocity differences to the sum of the squared magnitudes of the observed velocities, that is,

$$VDR = \frac{\sum |V_m - V_o|^2}{\sum |V_o|^2} \quad (1)$$

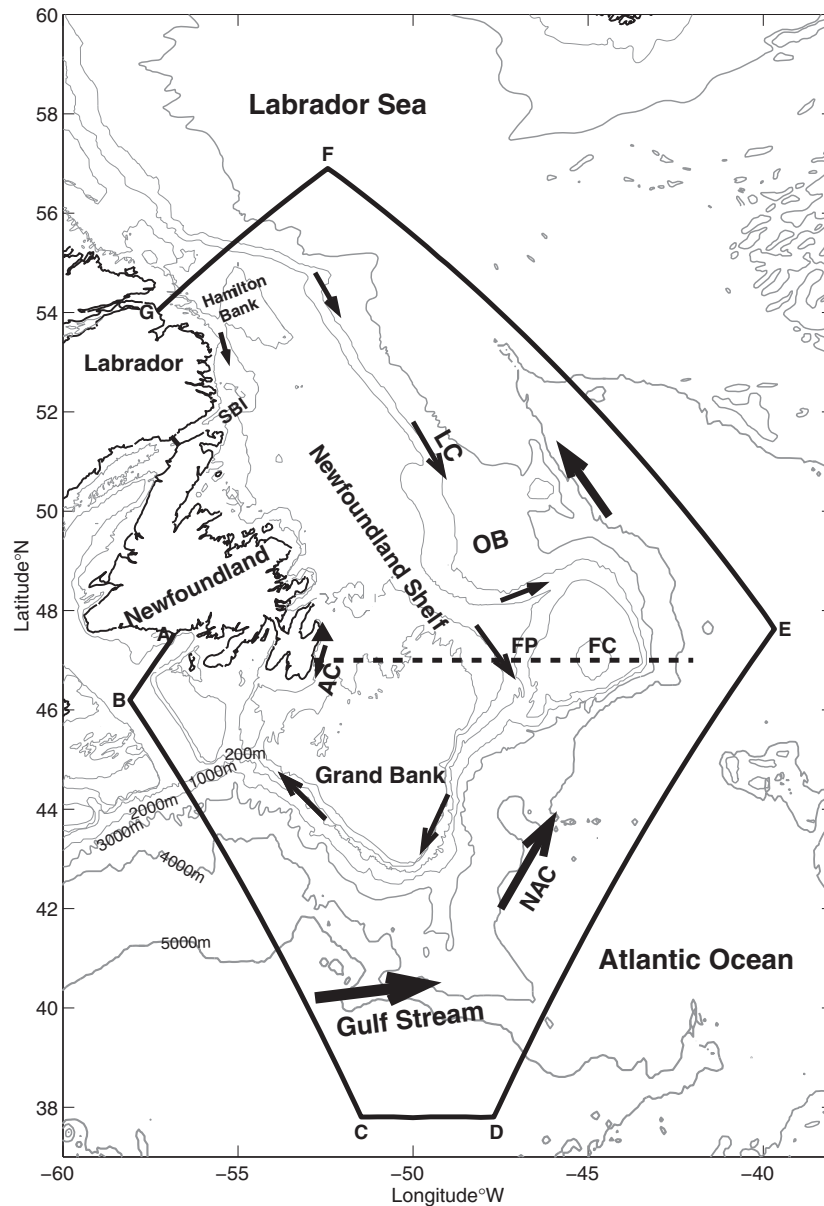


**Fig. 1.** Map showing the Newfoundland Shelf, the southern Labrador Shelf and adjacent NW Atlantic Ocean. The model open boundaries are shown in thick solid lines. The isobaths displayed are 100, 200, 1000, 3000, 4000, and 5000 m. The Flemish Cap (FC) transects are shown as thick dashed lines. AC: Avalon Channel; FP: Flemish Pass; LC: the Labrador Current; NAC: the North Atlantic Current; OB: Orphan Basin; SBI: Strait of Belle Isle. The solid triangle depicts the location of Station 27.

where  $V_m$  is the horizontal model velocity and  $V_o$  is the horizontal observational velocity. Lower VDR values indicate better agreement, with  $VDR = 0$  being the exact agreement.

### 3.1. Temperature and salinity comparison at Station 27

Station 27 (see Fig. 1) is located at 47.55°N and 52.59°W, with a water depth of 176 m. Hydrographic data were collected at this station dating back to 1946. Since late 1990s, temperature and salinity data at Station 27 have regularly been collected by the Northwest Atlantic Fisheries Centre through the Atlantic Zone Monitoring Program (AZMP) of Fisheries and Oceans Canada (<http://www.medsdmm.dfo-mpo.gc.ca/isdm-gdsi/azmp-pmza/index-eng.html>). In this study, the bi-weekly data from April to November 1999 are used to evaluate the model. The baseline prognostic model reproduces fairly the seasonal temperature evolution at different depths (Fig. 3). Near the surface the observed temperature increases about 14 °C from spring to summer. The observed RMS temperature variability is 8.5 °C. The correlation coefficient between the model and observed temperature is 0.95, the RMS difference 2.1 °C, and the mean difference is nearly −1.0 °C. The negative mean difference means that the model underestimates the observations. The RMS

(mean) difference in the mid-layer and near the bottom is between 0.4 (0.1) °C and 0.3 (0.1) °C, respectively. In summer, the model tends to underestimate near the surface.

The prognostic model reproduces approximately the thermocline evolution from spring to summer in response to the solar heating and wind changes (Fig. 4a and b). However, in July the model mixed layer depth is much less than the observed and the model stratification is not as sharp (Fig. 4b). The vertical sigma coordinate, rapid topographic changes and insufficient grid resolution may cause larger baroclinic pressure gradient error and lead to unrealistic upwelling at Station 27 and near the coast. Indeed, better agreement between the model and observed vertical structure is achieved away from the coast, as shown in Fig. 4c for a mid-shelf location (50°W and 47°N).

The surface salinity has a seasonal range of 1.5 psu, and the model-observation RMS difference is 0.3 psu. The bottom salinity does not change much seasonally, and the model reproduces the salinity well, with an RMS error of 0.1 psu. Although the present model does not explicitly consider the effects of precipitation and evaporation or freshening due to ice melting, they are implicitly accounted for through the restoration of the surface salinity at the synoptic time scale.

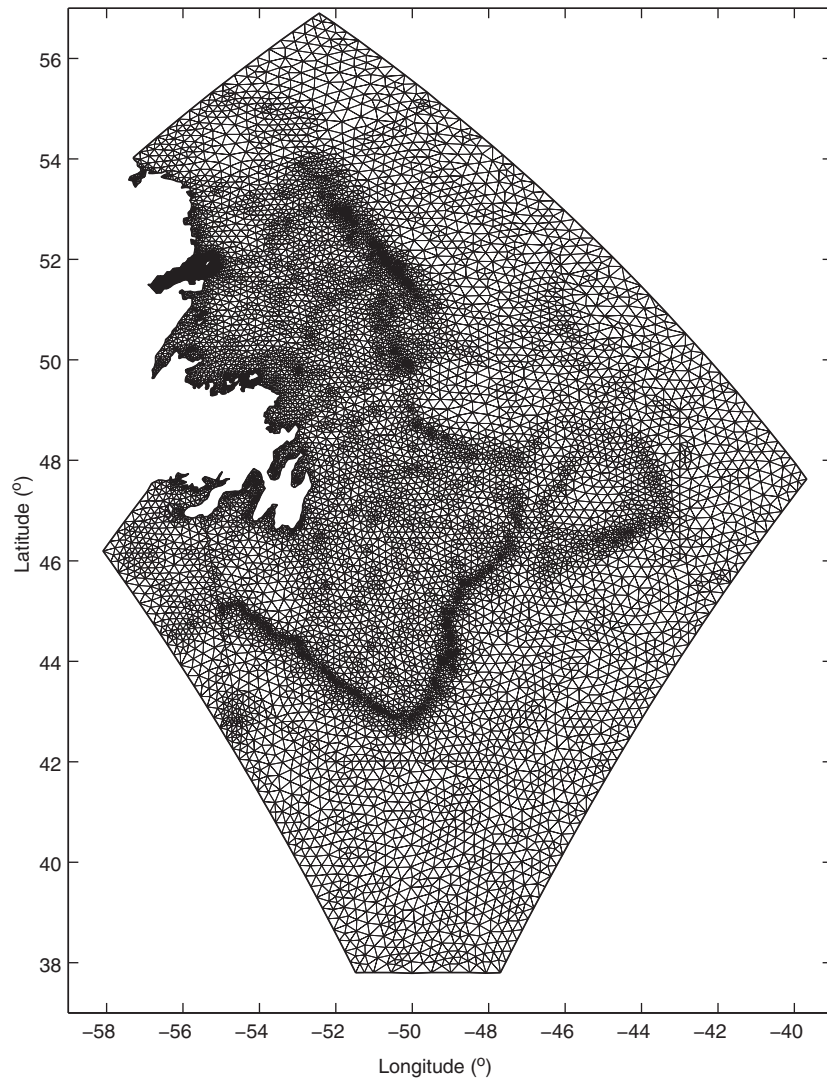
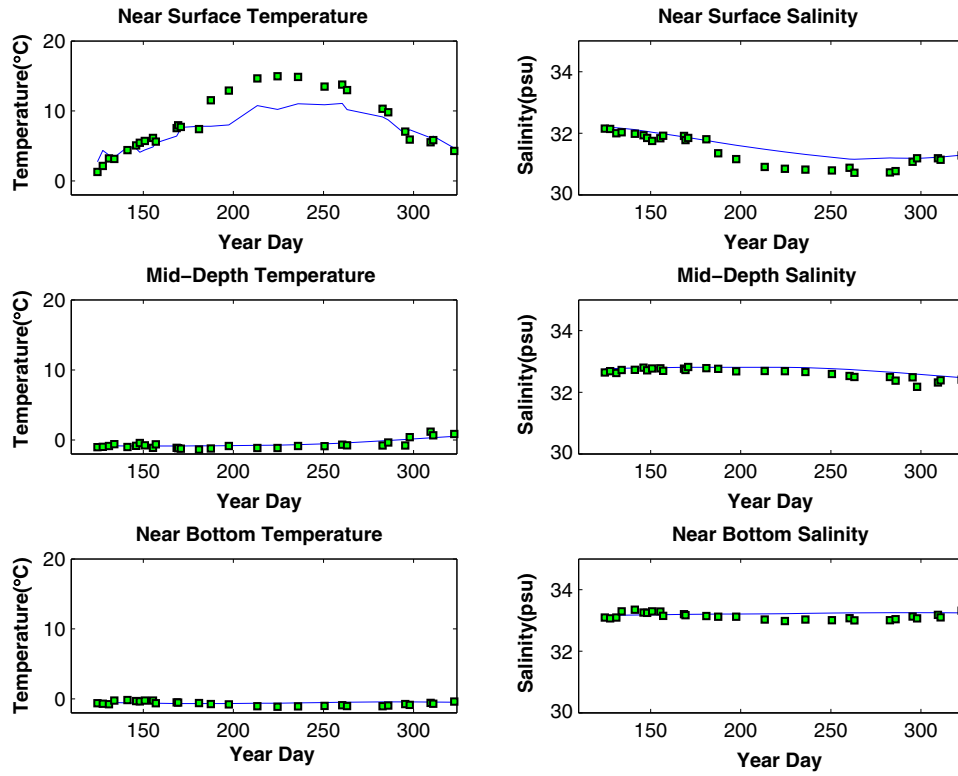
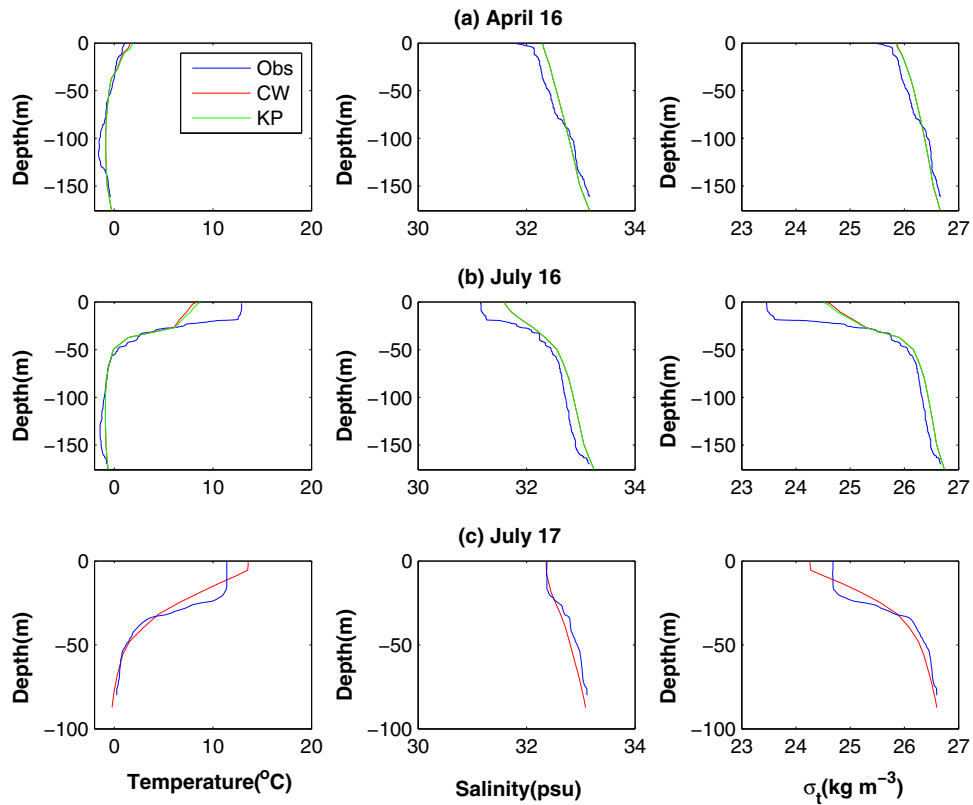


Fig. 2. The horizontal finite-element grid (slns2) used in the numerical model. The model origin is at 49.75°W 48.5°N. The grid is the same as that used in Han et al. (2008).



**Fig. 3.** Model (solid curve) and observed (square) temperature and salinity time series at Station 27 in 1999. The water depth at Station 27 is 176 m. Near surface: 0.8 m below the sea surface, mid-depth: 87.5 m; near bottom: 0.8 m above the bottom.



**Fig. 4.** Temperature, salinity and density profiles at Station 27 in (a) spring and (b) summer, and (c) at a mid-shelf location (50°W and 47°N) in summer. The location of Station 27 is indicated in Fig. 1. Blue: Observations; Red: baseline prognostic simulation with the CW scheme of the shortwave heat flux; Yellow: simulation with the KP scheme of the shortwave heat flux. (For interpretation of the references in color in this figure legend, the reader is referred to the web version of this article.)

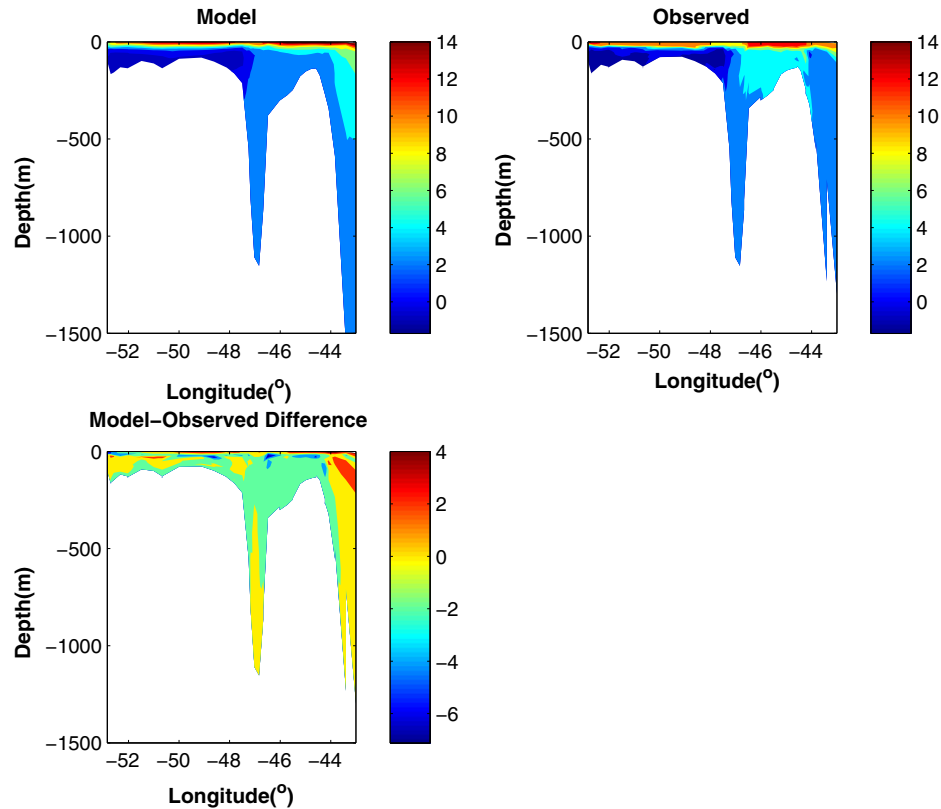


Fig. 5. Observed and modeled temperatures ( $^{\circ}\text{C}$ ) and their difference along the Flemish Cap transect on July 17–20, 1999.

### 3.2. Temperature and salinity comparison at the Flemish Cap transect

The AZMP program collects temperature and salinity data at the Flemish Cap transect at  $47^{\circ}\text{N}$ . The model solutions are compared with observed temperature (Fig. 5) and salinity (Fig. 6) on July 17–20, 1999. The model vertical structure qualitatively agrees well with observations. There are notable and localized temperature discrepancies, especially near the coast and shelf-edge. Over the entire transect, the observed temperature values vary from  $-1.5$  to  $13.1$   $^{\circ}\text{C}$ , and the salinity values from 31.3 to 34.9 psu. The mean temperature and salinity difference (model values minus observations) are 0.2 and  $-0.1$  psu. The RMS temperature and salinity differences are  $1.0$   $^{\circ}\text{C}$  and 0.2 psu.

### 3.3. Comparison with vessel-mounted ADCP currents

Vessel-mounted ADCP current data at the Flemish Cap transect on July 17–18, 1999 (Senciall et al., 2006) were detided using Han's (2000) tide model. The ADCP data were collected with the bottom tracking technology. There are no data in Flemish Pass for depths greater than 300 m. The ADCP data are simply grouped in cells of  $0.2^{\circ}$  in longitude and 10 m in depth, after which their mean is computed. The model output is interpolated to the mean measurement time and the center of cells.

There is good qualitative agreement between the present model and the ADCP measurements, in terms of the spatial distribution pattern and the current strength for the dominant southward current (Fig. 7). Both show the southward inshore and shelf-edge branches of the Labrador Current. There are also indication of recirculation and significant near-bottom flow. The RMS northward speed is 17.5 cm/s from the ADCP measurements and 15.0 cm/s from the model simulation. The velocity difference ratio accounting for both the eastward and northward components is 0.53, sug-

gesting general agreement but with significant discrepancy. Such general agreement for the instantaneous velocity comparison seems sufficient since currents from the vessel-mounted ADCP are difficult to derive and interpret and the model does not resolve all spatial and temporal scales. The quantitative agreement is much better at the climatological scale (see Section 5.2). Note that the statistics are calculated for water column below 20 m and above 150 m.

### 3.4. Temporal evolution and spatial structure of model circulation

The sub-surface model monthly-mean circulation (Fig. 8) is dominated by the equatorward flowing Labrador Current, similar to the climatological-monthly mean circulation pattern and consistent with previous model results (Tang et al., 1996; Han et al., 2008). The inshore and shelf-edge branches of the Labrador Current decrease slightly from April to May. The result also shows prominent offshore flow along the northern Grand Bank edge. An anti-cyclonic eddy is evident over the tail of the Grand Bank. The anti-cyclonic partial eddy is well defined over the Flemish Cap.

Near the surface, the wind-driven Ekman flow is important and shows strong synoptic-scale changes (Fig. 9). When the wind is primarily from the southwest, an eastward component from the wind-driven Ekman flow is evident. When the wind is dominantly from the west or northwest, the Ekman flow strengthens the overall southward flow over the Grand Bank.

We have calculated the volume transport at the Flemish Cap transect, through the Avalon Channel (from the coast to the 100-m isobath on the offshore side of the Avalon Channel, about 100 km from the coast) and through the Flemish Pass (from the 150-m isobath on the Grand Bank side to the 1000-m isobath on the Flemish Cap side), respectively (Fig. 10). The inshore Labrador Current through the Avalon Channel moves southward, but with

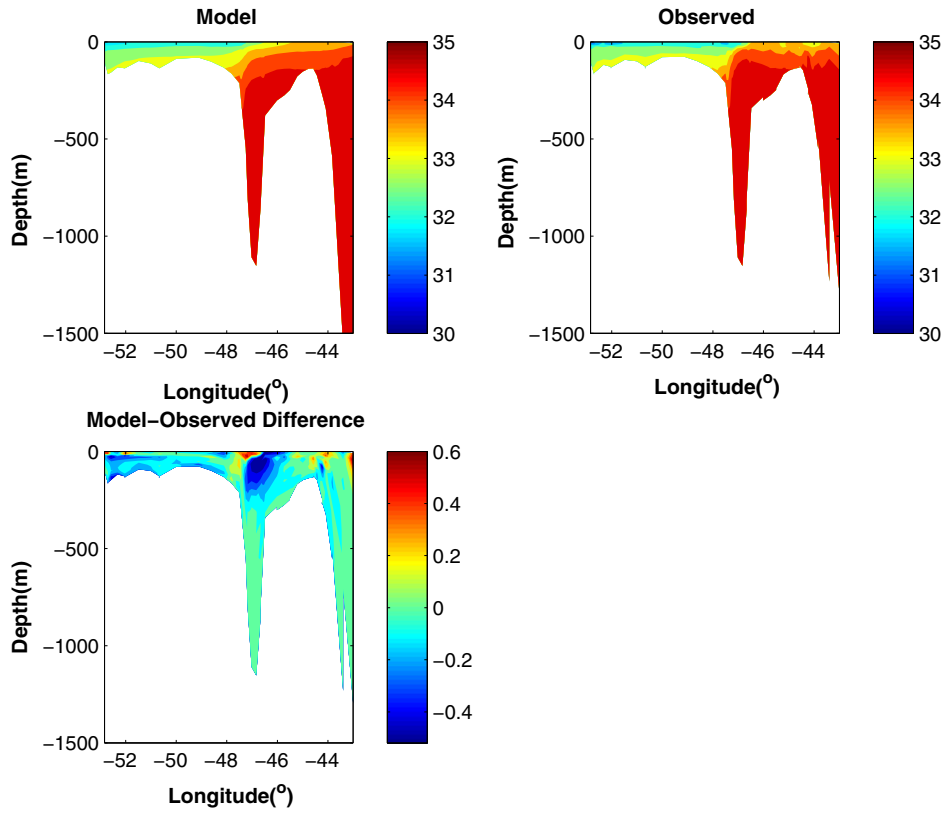


Fig. 6. Same as Fig. 5 but for salinity (psu).

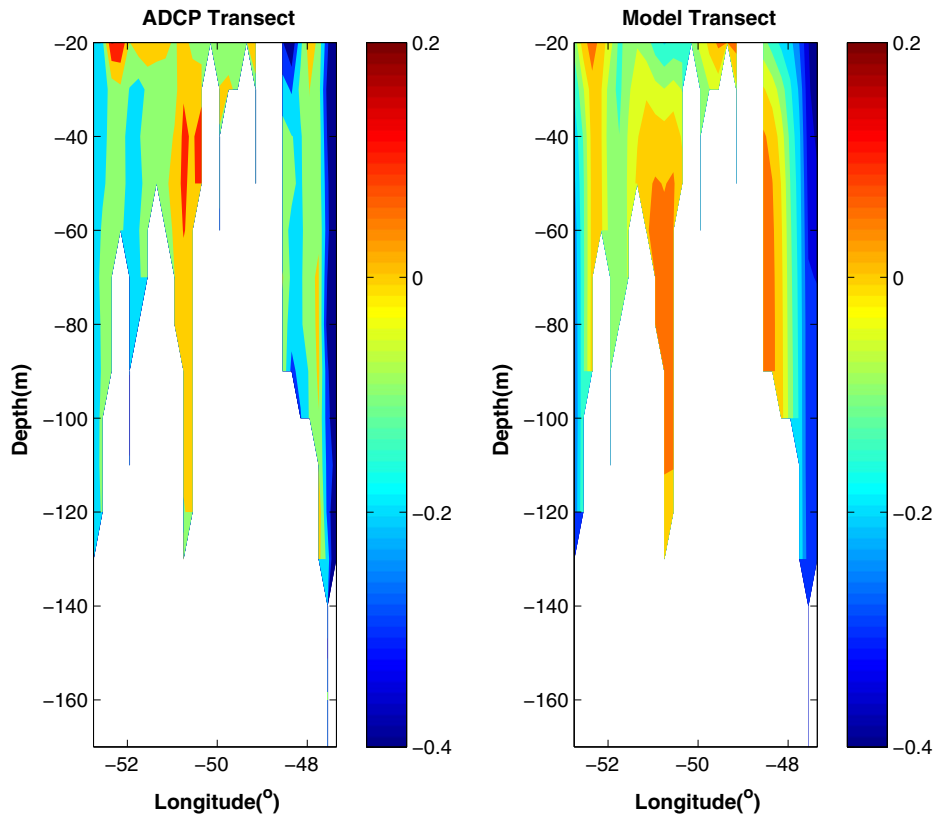
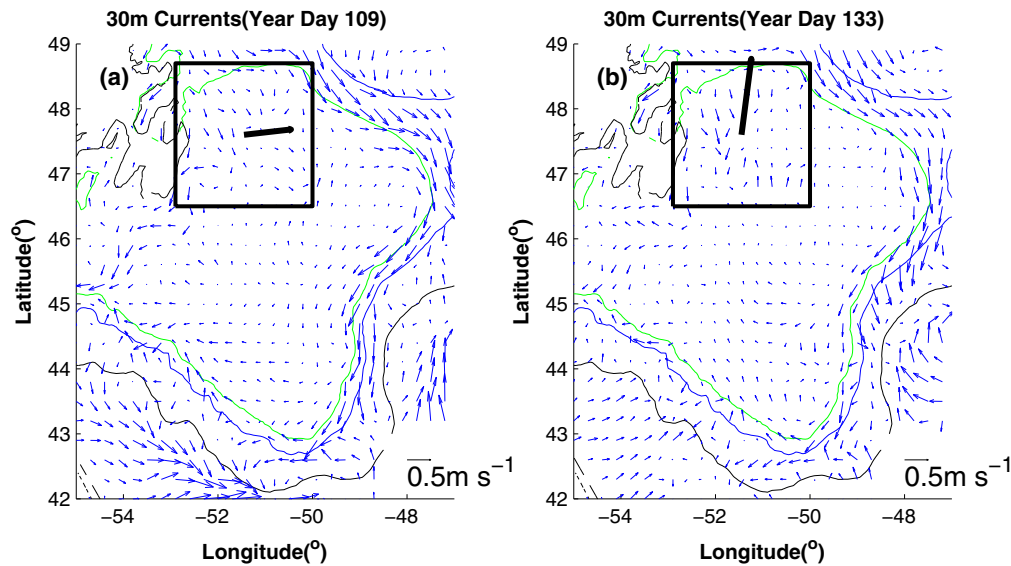
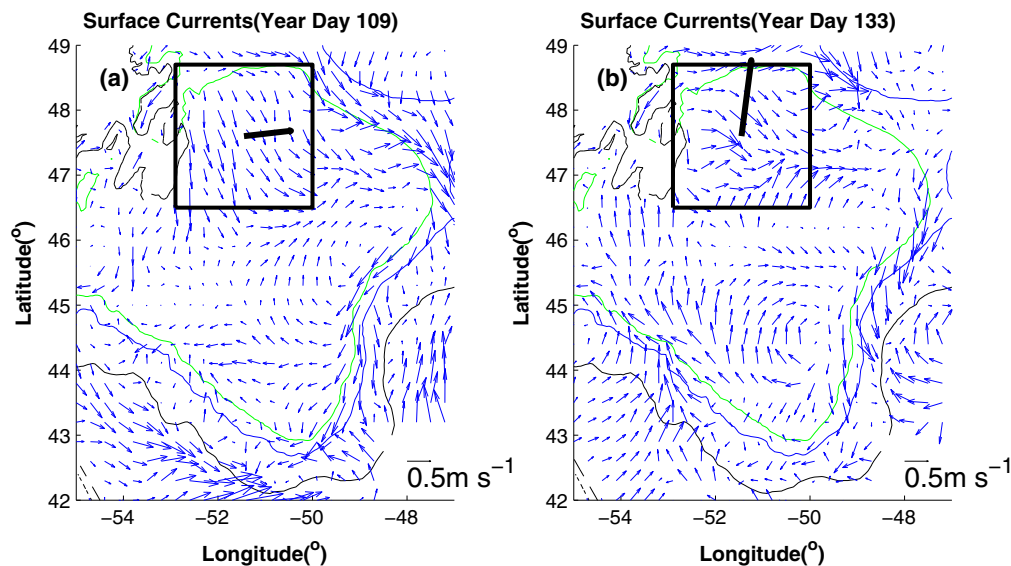


Fig. 7. Comparison of the model currents with vessel-mounted ADCP data along the Flemish Cap transect on July 17–18, 1999. Only the normal component (in  $m s^{-1}$ , positive northward) is shown.



**Fig. 8.** Subsampled model currents at 30 m. The 200-, 1000-, and 3000-m isobaths are also depicted. The thick black arrow depicts the direction of wind stress averaged inside the black square. The wind stress magnitude is 0.05 and 0.06 N/m<sup>2</sup> for Day 109 and 133, 1999.



**Fig. 9.** Same as Fig. 8, but at the surface.

occasional flow reversals. The mean southward transport is 0.8 Sv during the spring-fall period of 1999. The shelf-edge Labrador Current through the Flemish Pass is southward, with a spring-fall mean of 6.2 Sv. These values are comparable to previous observational and model estimates (Greenberg and Petrie, 1988; Han et al., 2008). The inshore and offshore Labrador Current both decrease from spring to summer and increase greatly towards fall, which are compatible with the seasonal evolution of the climatological monthly solutions. The present results are consistent with vessel-mounted ADCP observations and previous model simulations (Han et al., 2008).

### 3.5. Sensitivity to model parameterization

We have used an alternative short wave scheme (Kleeman and Power, 1995) to replace the baseline scheme of Curry and Webster (1999). Some differences in the model temperature can be seen at Station 27 (Fig. 4; CW for Curry and Webster and KP for Kleeman

and Power). The RMS near-surface temperature difference between the model and observations at Station 27 is 2.0 °C for Day 110–323, 1999. On the Flemish Cap transect, the model-observation RMS temperature difference is 1.1 °C on July 17–20, 1999. These differences are very close to those from the baseline CW scheme. These statistics suggest that the model temperature is not overly sensitive to the short wave schemes.

In the baseline model, the effect of the sea ice on salinity has been implicitly accounted for by restoring the sea surface salinity to the monthly-mean climatology. However, for the northern model domain, when there is significant ice coverage in spring, the model wind-driven near-surface currents may differ substantially from expected currents. This issue is left for future development of an FVCOM-based coupled ice-ocean model. In terms of the ice effect on the heat flux, we have conducted a proxy sensitivity experiment, in which we assume there is ice coverage north of 48°N in April and May, 1999 and take the albedo for the short-wave radiation to be 0.6. Compared with the baseline simulation,

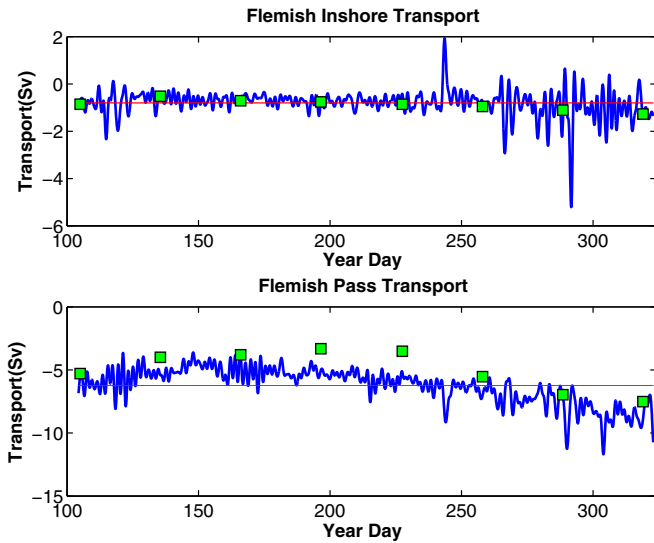


**Fig. 10.** Volume transport (blue, 36-h low-pass filtered) inshore and through the Flemish Pass at the Flemish Cap Transect (47°N) in 1999. The mean transport for the modeling period is also depicted (red). The volume transports from the climatological monthly-mean solutions are also shown (squares). (For interpretation of the references in color in this figure legend, the reader is referred to the web version of this article.)

this sensitivity simulation increases the RMS difference by 0.1 °C for both the near-surface temperature at Station 27 from April to November 1999 and the temperature at the Flemish Cap transect on July 17–20, 1999. Hence, the model temperature in the Grand Bank region seems not overly sensitive to whether or not the ice is explicitly included in the simulation.

#### 4. Validation of the baseline prognostic model at tidal time scales

The model solution is interpolated to observational locations for model-data comparisons. To provide a quantitative assessment of the model solution (for the tidal elevation and current), three measures were employed (Han et al., 2010): (1) The RMS difference between the observed amplitude and phase and the model solution for each constituent. (2) The average absolute RMS error (AbsErr),  $L^{-1}\sum_i D$ , and the relative RMS error (RelErr),  $L^{-1}\sum_i D/A_o$ , which are computed for semi-diurnal and diurnal constituents. The averaging is based on the total number ( $L$ ) of *in situ* observations either for tide and bottom pressure gauges or for current meter moorings.  $D$  is the RMS difference over a tidal cycle between model and observations, given by

$$D = \left[ \frac{1}{2} (A_o^2 + A_m^2) - A_o A_m \cos(\phi_o - \phi_m) \right]^{1/2} \quad (2)$$

where  $A$  and  $\phi$  are amplitudes and phases for a given constituent, and the subscripts  $m$  and  $o$  refer to model and observations respectively. (3) The root sum square (RSS) value (defined as the squared sum of the RMS differences of all five major constituents) for the tidal elevations.

Tidal elevation data are measured by coastal tide gauges and bottom pressure gauges and obtained from Han et al. (2010, see their Fig. 2 for locations). The observational dataset includes amplitude and phase for the five major semi-diurnal ( $M_2, S_2, N_2$ ) and diurnal constituents ( $K_1, O_1$ ). The tidal current data for the five tidal constituents are obtained from the Northwest Atlantic tidal current database (Drozdowski et al., 2002). The database consists of ti-

dal current data stored as eastward (U) and northward (V) components of amplitude and Greenwich phase lag (see Han et al.'s (2010) Fig. 3 for locations).

#### 4.1. Tidal elevation comparison

The FVCOM co-tidal charts for  $M_2$  and  $K_1$  (Fig. 11) are consistent with previous results based on tide-gauge observations (Godin, 1980), basin-scale (Egbert and Erofeeva, 2002) models, and inter-regional (Dupont et al., 2002; Han et al., 2010) simulations. The tidal results show an overall southward (and anticlockwise) propagation with the amplitude increasing from the deep ocean toward the Newfoundland Labrador coast.

The model computed elevations are compared with the observed values for the semi-diurnal and diurnal constituents respectively. The statistics (Table 1) indicate that the computed tidal elevations are in good agreement with observations. The root-sum-square absolute error for the five tidal constituents is 4 cm. The accuracy of the present model is comparable to Han et al.'s (2009) and better than Dupont et al.'s (2002). The former assimilated multi-satellite tides into a 3-D barotropic model and the latter assimilated TOPEX/Poseidon crossover tides into a 2-D model.

#### 4.2. Tidal currents comparison

On the Labrador shelf, the computed  $M_2$  tidal current (Fig. 12a) is small, except on the inner shelf region. Over Hamilton Bank the current magnitudes are  $\sim 5$  cm/s. Computed  $K_1$  currents (Fig. 12b) show localized intensification. The localized diurnal current intensification may be related to the occurrence of a first-mode shelf wave at the  $K_1$  frequency. The intensification is expected to be strongly dependent on the bottom topography, and so high-resolution and accurate topography is crucial in obtaining accurate diurnal currents.

On the Newfoundland Shelf, the model  $M_2$  tidal current is rectilinear along the coast of Avalon Peninsula, and more circular over the Grand Banks (Fig. 12a). Stronger tidal currents occur (up to 20–30 cm/s) in the outer-shelf and shelf-break areas. The computed  $K_1$  surface current (Fig. 12b) is weaker overall, however, featuring localized intensification associated with the resonance of the first-mode shelf wave (Han, 2000) over the northeastern Grand Bank and Slope, the Flemish Cap and a few other areas.

The model tidal currents are compared with observations for the  $M_2$  and  $K_1$  constituents. In general, the relative error in an area with weak to moderate tidal currents, such as the Labrador and Newfoundland Shelf, is expected to be large. The scatter plots (not shown) for the amplitude and phase for eastward and northward components of  $M_2$  and  $K_1$  constituents indicate that the model currents are in better agreement with observations for the semi-diurnal constituents than for the diurnal ones. As expected, while the absolute difference is small, the relative error is generally large (Table 2) since tidal currents in the model domain are weak. The relative errors of the model 3-D tidal currents are of the order 50% for the semi-diurnals, and larger for the diurnals. The larger diurnal discrepancy is clearly related to the localized intensification of the  $K_1$  currents north of the Flemish Pass (Figs. 11b and 12b). An increase of the horizontal grid resolution in the area does not mitigate the overestimation. In contrast, the localized intensification occurred in Han's (2000) finite-difference simulation (with a  $1/6^\circ$  by  $1/6^\circ$  resolution) and Han et al.'s (2010) finite-difference assimilative model (with a  $1/12^\circ$  by  $1/12^\circ$  resolution), inshore of the present intensification location, agrees well with observations. The shift of the intensification seems to be peculiar to the unstructured grid mesh and might be a manifestation of the bathymetric error in the high-resolution grid through the shelf wave.

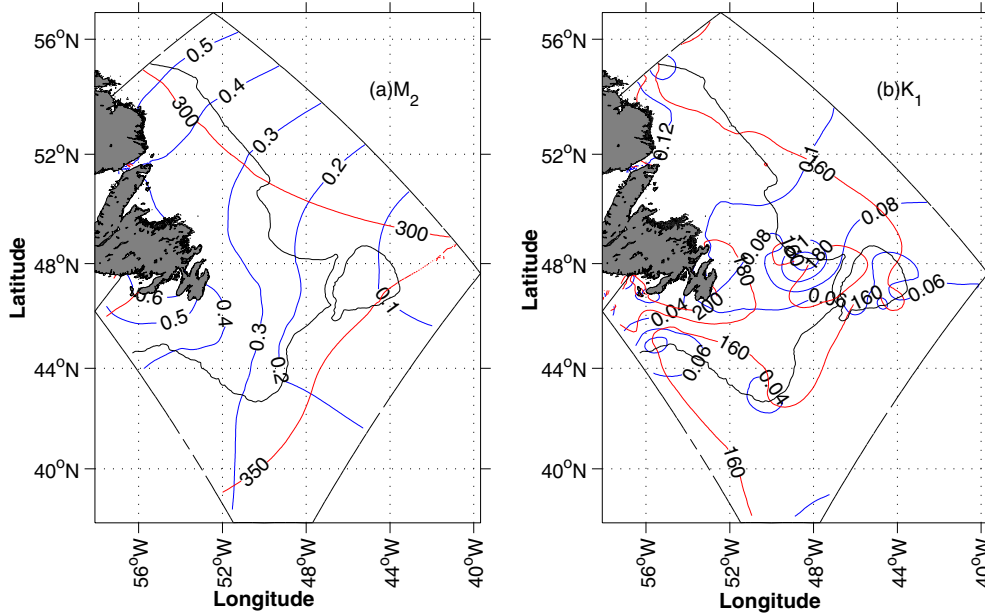


**Fig. 11.** Co-tidal charts (a)  $M_2$  (b)  $K_1$ . Amplitude (blue) is in meters and phase (red) is in degrees (Greenwich phase lag). The 3000-m isobath is also depicted (gray). (For interpretation of the references in color in this figure legend, the reader is referred to the web version of this article.)

**Table 1**  
 Statistics from the comparison between observed and model tidal elevations over the Newfoundland and Labrador Shelf and Slope. RMSD: root-mean-square difference.

	RMSD Amp (cm)	RMSD phase (°)	AbsErr (cm)	RelErr (%)	# of Points
$M_2$	3.7	3.9	2.4	6.7	42
$S_2$	1.9	5.7	1.4	9.3	42
$N_2$	1.8	8.7	1.2	15.2	42
$K_1$	2.4	25.7	2.2	28.9	42
$O_1$	1.5	15.1	1.3	22.0	42

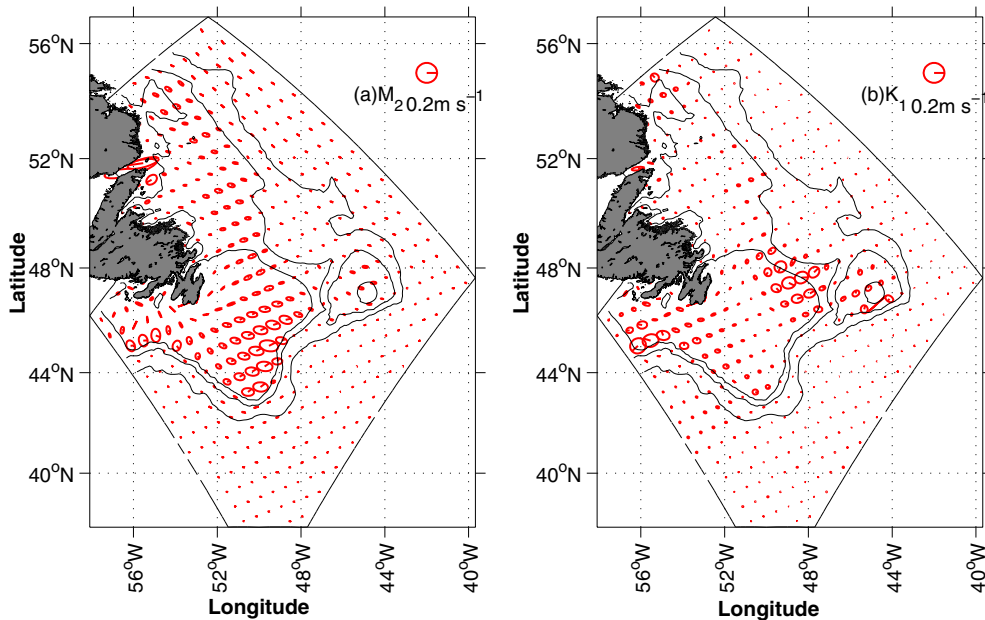


**Fig. 12.** Subsampled tidal ellipses for  $M_2$  and  $K_1$  at the surface. The 200-, 1000-, and 3000-m isobaths are also depicted (gray).

In general, the statistics indicate the present tidal simulation has comparable overall accuracy to that of Han et al.'s (2010) data-assimilative finite-difference model for the Grand Banks of Newfoundland and the southern Labrador Shelf. The general

good results for tidal elevations and currents from the present FVCOM model may be attributed to the specification of better tidal elevation at the open boundary and the inclusion of non-tidal dynamics.

**Table 2**

Statistics from the comparison between observed and model tidal currents over the Newfoundland and Labrador Shelf and Slope.

	RMSD U Amp (cm s <sup>-1</sup> )	RMSD U Phase (°)	RMSD V Amp (cm s <sup>-1</sup> )	RMSD V Phase (°)	RelErr U %	RelErr V %	# of points
M <sub>2</sub>	1.5	41.0	1.8	66.2	47.0	50.2	109
S <sub>2</sub>	0.7	49.0	0.9	75.3	45.1	56.2	57
N <sub>2</sub>	0.6	53.0	0.9	67.8	54.9	52.8	49
K <sub>1</sub>	6.1	90.0	5.5	78.8	180.0	180.0	44
O <sub>1</sub>	2.8	104.2	2.3	75.1	156.0	104.0	47

**Table 3**

Statistics (VDR and correlation) from the comparison between observed and model monthly-mean currents over the Newfoundland and Labrador Shelf and Slope. Values for Han et al.'s (2008) finite element model are also shown for comparison. All selected velocity data have magnitude of greater than or equal to 0.02 m/s.

Month	Number of points	VDR		Correlation	
		Han et al. (2008)	FVCOM	Han et al. (2008)	FVCOM
January	111	0.76	0.34	0.69	0.80
February	99	0.57	0.28	0.76	0.84
March	93	0.52	0.27	0.71	0.84
April	82	1.13	0.75	0.56	0.67
May	92	0.70	0.66	0.62	0.68
June	117	0.47	0.48	0.73	0.72
July	169	0.56	0.56	0.68	0.68
August	183	0.71	0.59	0.61	0.67
September	169	0.48	0.39	0.73	0.78
October	127	0.51	0.35	0.70	0.78
November	93	0.35	0.19	0.80	0.88
December	114	0.49	0.32	0.75	0.80

## 5. Validation of climatological monthly-mean models

In this section we compare the FVCOM climatological monthly-mean solutions (see Section 2.3) with Han et al.'s (2008) climatological monthly-mean finite-element solutions. The FVCOM monthly-mean solutions are obtained using the same open boundary conditions for the monthly-mean sea level, temperature and salinity, the same initial conditions for temperature and salinity, and the same monthly-mean wind stresses at the sea surface. As such, they can be compared with Han et al.'s (2008) robust diagnostic finite-element model results.

The FVCOM monthly-mean solutions clearly indicate dominant nearshore and shelf-edge branches of the Labrador Current and cross-shelf exchanges. The currents are stronger in fall than spring/summer. Overall, the FVCOM solutions are in good qualitative agreement with observational features shown in Han et al.'s (2008).

### 5.1. Evaluation against current meter data

The FVCOM and Han et al.'s (2008) model currents are evaluated against the same moored current measurements using the method described in Section 3. Observed monthly-mean currents were estimated from a database at the Bedford Institute of Oceanography (Gregory and Bussard, 1996), for months with a minimum of 20 days of data. Note that each mooring site usually has observations at one to three depths (positions in the vertical) within one or two years. The statistics for each month are summarized in Table 3. It can be seen that the FVCOM solution has better agreement with observations in all months (Table 3). Compared with Han et al.'s (2008) robust diagnostic model, the present model ensures local mass conservation and allows full prognostic adjustment of temperature and salinity.

### 5.2. Assessment against ADCP data

Following Han et al. (2008), we compared the FVCOM model results with the multi-year mean currents of de-tided vessel-mounted ADCP data at the Flemish Cap transect.

We calculate statistics for the model and observed currents between the 20- and 150-m depths. In April, the RMS speed is 16.9 and 16.1 cm/s, with an RMS difference of 6.6 cm/s. In July the RMS model and ADCP speed is 11.5 and 13.1 cm/s, with an RMS difference of 7.9 cm/s. In November, the RMS speed is 25.8 and 17.1 cm/s from the model and ADCP, with an RMS difference of 8.0 cm/s. The velocity difference ratio is 0.22. The velocity difference ratios are 0.16, 0.34, and 0.22 in April, July and November, respectively. Therefore, there is generally good agreement between the model and ADCP data for spring through fall. While the overall agreement is best in April, the model reproduces the shelf-edge Labrador Current best in November. The model underestimates the shelf-edge current in April and summer. These statistics indicate that the present FVCOM model produces better agreement with ADCP observations than does the Han et al.'s (2008) finite element model. Note that the statistics are calculated for water column below 20 m and above 150 m.

## 6. Concluding remarks

We have developed a 3-D, unstructured-grid, prognostic ocean circulation model for the Grand Banks of Newfoundland. The prognostic model is based on the FVCOM circulation model and forced by winds, heat flux, tides and large-scale climatological monthly-mean inflows at the open boundaries. The model results have been evaluated against tide-gauge and bottom pressure gauge, CTD, current meter, and vessel-mounted ADCP data.

The present model provides a new capability for simulating synoptic-scale ocean variability using the unstructured grid ocean model for this region. Detailed comparison of the prognostic model circulation with vessel-mounted ADCP data indicates approximate agreement with observations (a VDR of 0.53) at the Flemish Cap transect on July 17–18, 1999. The model is able to reproduce the surface temperature with an RMS error of 2.1 °C and the surface salinity with an RMS error of 0.3 psu at Station 27 from April to November, 1999. The temperature and salinity have an accuracy of 1.0 °C and 0.2 psu at the Flemish Cap transect on July 17–20, 1999. The prognostic model results indicate significant synoptic and spatial variations in the regional circulation. The region is

dominated by the equatorward Labrador Current along the shelf edge and along the Labrador and Newfoundland coasts. The near-surface circulation is substantially influenced by the wind on the synoptic scale. With the dominant winds from the west-northwest in the early spring to southwest in late spring and summer, the surface current over the Grand Bank reinforces the southward density driven current in the early spring but increases eastward flow in the late spring and summer.

Model tidal elevations are in good (RSS absolute error of 4 cm for the five major constituents) agreement with observations and comparable or better than other models developed in the past decade. The model can approximately simulate tidal currents, except for localized overestimation of the diurnal currents north of the Flemish Pass.

The FVCOM model shows overall good skill in reproducing climatological monthly-mean currents. The FVCOM model has notably better agreement with observations than Han et al.'s (2008) robust diagnostic finite-element model, as a result of improved numerical schemes and full prognostic adjustment in the FVCOM.

The present study clearly demonstrates the ability of the FVCOM-based circulation model, while pointing to potential avenues of further improvement. First, the present model reproduces the temperature and salinity quite well in spring and early summer. Nevertheless, the model tends to underestimate the upper-layer temperature near the coastal upwelling zone (e.g. Station 27) in summer. Improved nearshore bathymetry, higher spatial resolution, and a hybrid vertical coordinate could lead to more accurate simulation of coastal upwelling and therefore of the vertical temperature and salinity structure near the coast. Second, the offshore open boundary is on the offshore edge of the Gulf Stream and the North Atlantic Current, which could limit adequate adjustment to the climatological monthly boundary conditions and thus affect interactions between the Labrador Current and the Gulf Stream/North Atlantic Current. Our specification of the monthly climatological temperature and salinity values along these boundaries should mean that the foregoing currents are represented reasonably well, at least in an average sense. The resolution of the climatology and the way in which it was computed (e.g., how much smoothing) has probably made the fronts less sharp, but all these currents should be there. In future studies, we may move some of the open boundaries further offshore or specify open boundary conditions based on eddy-resolving large scale ocean model output. Third, the present model applies a simple nudging technique of temperature and salinity. This seems to well serve the present purpose of validating the new modeling technique for the synoptic-scale variability. Nevertheless, more advanced nudging schemes (e.g., Sheng et al., 2001) could be implemented. Fourth, a coupled ice-ocean model could explicitly account for effects of ice formation, melting and advection, and may improve overall agreement of the temperature, salinity and circulation.

## Acknowledgments

We thank Dr. Changsheng Chen for providing the FVCOM code and the AZMP Program of Fisheries and Oceans Canada for making hydrographic data available online. Helpful comments were received from the two Ocean Modeling reviewers. This work has been partially funded by the ArcticNet, a Network of Centres of Excellence of Canada, and by the Centre for Ocean Model Development and Application, Fisheries and Ocean Canada.

## References

- Chen, C.R., Liu, H., Beardsley, R.C., 2003. An unstructured grid, finite volume primitive equation coastal ocean model: application to coastal ocean and estuaries. *J. Atmos. Ocean. Technol.* 20, 159–186.
- Chen, C., Beardsley, R., Cowles, G., 2006. An unstructured grid, finite-volume coastal ocean model. FVCOM User Manual, second ed., 315pp.
- Curry, J.A., Webster, P.J., 1999. *Thermodynamics of Atmospheres and Oceans*, first ed., 65. Academic Press, 471pp.
- Drozdowski, A., Hannah, C.G., Loder, J.W., 2002. The Northwest Atlantic tidal current database. Tech. rep., BIO, Department of Fisheries and Oceans, Bedford Institute of Oceanography, P.O. Box 1006, Dartmouth, NS, Canada, B2Y-4A2.
- Dupont, F., Hannah, C.G., Greenberg, D.A., Cherniawsky, J.Y., Naime, C.E., 2002. Modelling system for tides. *Can. Tech. Rep. Hydrogr. Ocean Sci.* 221, vii + 72 pp.
- Egbert, G.D., Erofeeva, S., 2002. Efficient inverse modeling of barotropic ocean tides. *J. Atmos. Ocean. Technol.* 19, 183–204.
- Fairall, C.W., Bradley, E.F., Rogers, D.P., Edson, J.B., Young, G.S., 1996. Bulk parameterization of air-sea fluxes for COARE. In: *The 8th Conference on Air-Sea Interaction/Conference on the Global Ocean-Atmosphere-Land System (GOALS)*, Atlanta, GA.
- Fung, I.Y., Harrison, D.E., Lacs, A.A., 1984. On the variability of the net long-wave radiation at the ocean surface. *Rev. Geophys. Space Phys.* 22 (2), 177–193.
- Geshelin, Y., Sheng, J., Greatbatch, R.J., 1999. Monthly mean climatologies of temperature and salinity in the western North Atlantic. *Can. Tech. Rep. Hydrogr. Ocean Sci.* 153, 62.
- Godin, G., 1980. Cotidal charts for Canada. *Manuscr. Rep. Ser.*, vol. 55. Mar. Sci. Dir., Dept. Fish. and Oceans, Ottawa, Ontario, Canada, 93pp.
- Gregory, D.N., Bussard, C., 1996. Current statistics for the Scotian Shelf and slope. *Can. Data Rep. Hydrogr. Ocean Sci.* 144, iv + 167pp.
- Greenberg, D.A., Petrie, B.D., 1988. The mean barotropic circulation on the Newfoundland shelf and slope. *J. Geophys. Res.* 93, 15541–15550.
- Han, G., 2000. Three-dimensional modeling of tidal currents and mixing quantities over the Newfoundland Shelf. *J. Geophys. Res.* 105, 11407–11422.
- Han, G., 2005. Wind-driven barotropic circulation off Newfoundland and Labrador. *Continental Shelf Res.* 25, 2084–2106.
- Han, G., Kulka, D., 2009. Dispersion of eggs, larvae and pelagic juveniles of white hake (*Urophycis tenuis*) in relation to ocean currents of the Grand Bank: a modelling approach. *J. of Northwest Atlantic Fishery Science* 41, 183–196.
- Han, G., Loder, J.W., Smith, P.C., 1999. Seasonal-mean hydrography and circulation in the Gulf of St. Lawrence and eastern Scotian and southern Newfoundland shelves. *J. Phys. Oceanogr.* 29 (6), 1279–1301.
- Han, G., Lu, Z., Wang, Z., Helbig, J., Chen, N., deYoung, B., 2008. Seasonal variability of the Labrador Current and shelf circulation off Newfoundland. *J. Geophys. Res.* 113, C10013. doi:10.1029/2007JC004376.
- Han, G., Paturi, S., deYoung, B., Yi, S., Shum, C.-K., 2010. A 3-D data-assimilative tide model of Northwest Atlantic. *Atmosphere-Ocean* 48, 39–57.
- Kleeman, R., Power, S.B., 1995. A simple atmospheric model of surface heat flux for use in ocean modeling studies. *J. Phys. Ocean.* 25, 92–105.
- Li, J., Scinocca, J., Lazare, M., McFarlane, N., von Salzen, K., Solheim, L., 2006. Ocean surface albedo and its impact on radiation balance in climate model. *J. Climate* 19, 6314–6333.
- Loder, J.W., Han, G., Hannah, C.G., Greenberg, D.A., Smith, P.C., 1997. Hydrography and baroclinic circulation in the Scotian Shelf region: Winter versus summer. *Can. J. Fish. Aquat. Sci.* 54, 40–56. doi:10.1139/cjfas-54-S1-40.
- Monahan, E.C., MacNiocaill, G., 1986. *Oceanic Whitecaps and their Role in Air-Sea Exchange Processes*. Springer-Verlag, New York, LLC, 312pp.
- Pawlowicz, R., Beardsley, R., Lentz, S., Deverm, E., Anis, A., 2001. The air-sea toolbox: boundary-layer parameterization for everyone. *EOS, Trans. Am. Geophys. Union* 84 (1), 2.
- Pepin, P., Helbig, J.A., 1997. Distribution and drift of Atlantic cod (*Gadus morhua*) eggs and larvae on the northeast Newfoundland shelf. *Can. J. Fish. Aquat. Sci.* 54, 670–685.
- Senciall, D., Chen, N., Cobourne, E., Han, G., Loder, J., 2006. ADCP currents along the Flemish Cap Transect, The National Science Workshop, Fisheries and Oceans Canada, Mont-Joli, Quebec.
- Sheng, J., Greatbatch, R.J., Wright, D., 2001. Improving the utility of ocean circulation models through adjustment of the momentum balance. *J. Geophys. Res.* 106, 16711–16728.
- Tang, C.L., Gui, Q., Peterson, I.K., 1996. Modeling the mean circulation of the Labrador Sea and the adjacent shelves. *J. Phys. Oceanogr.* 26, 1989–2010.
- Yao, T., Tang, C.L., Peterson, I.K., 2000. Modeling the seasonal variation of sea ice in the Labrador Sea with a coupled multicategory ice model and the Princeton ocean model. *J. Geophys. Res.* 105 (C1), 1153–1165. doi:10.1029/1999JC900264.
- Zhang, H.-M., Bates, J.J., Reynolds, R.W., 2006. Assessment of composite global sampling: sea surface wind speed. *Geophys. Res. Lett.* 33, L17714. doi:10.1029/2006GL027086.
- Zhang, S., Sheng, J., Greatbatch, R., 2004. A coupled ice-ocean modeling study of the northwest Atlantic Ocean. *J. Geophys. Res.* 109, C04009. doi:10.1029/2003JC001924.